Cell

Coding-Independent Regulation of the Tumor Suppressor PTEN by Competing Endogenous mRNAs

Yvonne Tay,[1] Lev Kats,[1] Leonardo Salmena,[1] Dror Weiss,[1] Shen Mynn Tan,[2,3] Ugo Ala,[1,4] Florian Karreth,[1] Laura Poliseno,[1,6] Paolo Provero,[4] Ferdinando Di Cunto,[4] Judy Lieberman,[2,3] Isidore Rigoutsos,[5] and Pier Paolo Pandolfi[1,*]

[1]Cancer Genetics Program, Division of Genetics, Beth Israel Deaconess Cancer Center, Department of Medicine and Pathology, Beth Israel Deaconess Medical Center

[2]Immune Disease Institute and Program in Cellular and Molecular Medicine, Children's Hospital Boston

[3]Department of Pediatrics

Harvard Medical School, Boston, MA 02115, USA

[4]Molecular Biotechnology Center and Department of Genetics, Biology, and Biochemistry, University of Turin, Turin, Italy

[5]Computational Medicine Center, Jefferson Medical College, Thomas Jefferson University, Philadelphia, PA 19107, USA

[6]Present address: Department of Dermatology, New York University School of Medicine, 522 First Avenue, Smilow 406, New York, NY 10016, USA

*Correspondence: ppandolf@bidmc.harvard.edu

DOI 10.1016/j.cell.2011.09.029

SUMMARY

Here, we demonstrate that protein-coding RNA transcripts can crosstalk by competing for common microRNAs, with microRNA response elements as the foundation of this interaction. We have termed such RNA transcripts as competing endogenous RNAs (ceRNAs). We tested this hypothesis in the context of PTEN, a key tumor suppressor whose abundance determines critical outcomes in tumorigenesis. By a combined computational and experimental approach, we identified and validated endogenous protein-coding transcripts that regulate PTEN, antagonize PI3K/AKT signaling, and possess growth- and tumor-suppressive properties. Notably, we also show that these genes display concordant expression patterns with *PTEN* and copy number loss in cancers. Our study presents a road map for the prediction and validation of ceRNA activity and networks and thus imparts a *trans*-regulatory function to protein-coding mRNAs.

INTRODUCTION

Regulation of gene expression by small noncoding RNA molecules is ubiquitous in many eukaryotic organisms from protozoa to plants and animals. In mammals, ~22 nucleotide long RNAs termed microRNAs guide the RNA-induced silencing complex (RISC) to microRNA response elements (MREs) on target transcripts, usually resulting in degradation of the transcript or inhibition of its translation (Bartel, 2009; Bartel and Chen, 2004). Individual genes often contain MREs for multiple distinct microRNAs, and conversely, individual microRNAs often target multiple distinct transcripts (Friedman et al., 2009).

We and others recently provided experimental support to the hypothesis that RNA molecules that share MREs can regulate each other by competing for microRNA binding (Cazalla et al., 2010; Jeyapalan et al., 2011; Kloc, 2008; Lee et al., 2009; Poliseno et al., 2010b; Seitz, 2009). Specifically, we reported several examples of pseudogene transcripts exerting regulatory control of their ancestral cancer gene's expression levels by competing for microRNAs that targeted sequences common to the mRNA and the pseudo-mRNA (Poliseno et al., 2010b), in keeping with the notion that the microRNA activity should be theoretically affected by the availability of its target MRE in the cellular milieu (Arvey et al., 2010).

This, in turn, led us to hypothesize that the mRNA/microRNA network would operate through a reverse logic whereby protein-coding and noncoding mRNAs would communicate with each other in a microRNA-dependent manner through a MRE language (Salmena et al., 2011). We proposed that a reversed RNA→microRNA function exists, whereby RNAs actively regulate each other through direct competition for microRNA binding. In this work, we tested this hypothesis experimentally and present a comprehensive scheme for the prediction and validation of ceRNA activity and networks demonstrating that bioinformatic predictions followed by a set of stringent biological tests allow for the identification and validation of ceRNAs for mRNAs of interest. We focused our analysis on the ceRNA network encompassing PTEN, a critical tumor suppressor gene that encodes a phosphatase that converts phosphatidylinositol 3,4,5-trisphosphate to phosphatidylinositol 4,5-bisphosphate, thereby antagonizing the highly oncogenic PI3K/Akt-signaling pathway (Hollander et al., 2011).

PTEN was selected as a model system for three reasons: (1) PTEN expression is frequently altered in a wide spectrum of human cancers (Hollander et al., 2011), (2) subtle changes in

PTEN dose dictate critical outcomes in tumor initiation and progression in vivo (Alimonti et al., 2010; Berger et al., 2011; Trotman et al., 2003), and (3) numerous microRNAs have been validated as PTEN regulators, including the proto-oncogenic miR-106b~25 cluster that is overexpressed in prostate cancer (Huse et al., 2009; Mu et al., 2009; Olive et al., 2009; Poliseno et al., 2010a; Xiao et al., 2008). Taken together, these previous studies suggested that bona fide PTEN ceRNAs, as well as a broader PTEN ceRNA network, may represent a previously uncharacterized RNA-dependent tumor-suppressive dimension.

RESULTS

Identification of Candidate PTEN ceRNAs

To identify and characterize the PTEN ceRNA network in the human genome, we devised a multifaceted scheme involving integrated computational analysis and experimental validation (Figure 1A), an approach that we termed *mu*tually *ta*rgeted *M*RE enrichment (MuTaME). Initially, we sought to identify mRNAs that are targeted by *PTEN*-targeting microRNAs. We focused on validated *PTEN*-targeting microRNAs, specifically those previously implicated in the ceRNA-mediated regulation of PTEN by its pseudogene *PTENP1*: miR-17-5p, miR-19a, miR-19b, miR-20a, miR-20b, miR-26a, miR-26b, miR-93, miR-106a, miR-106b, and miR-214 (Poliseno et al., 2010a, 2010b), and we excluded miR-214 from subsequent analysis, as it is not expressed in the cell lines utilized to validate the putative PTEN ceRNAs (Figure S1A available online).

Importantly, we also examined the physical association of the *PTEN* 3′UTR with endogenous levels of these microRNAs in the cell line used in our study. We reasoned that this represents a critical selective criterion to guide the computational component of our analysis (Figure 1A). To do so, we performed RNA immunoprecipitation (RIP) to pull down endogenous microRNAs associated with the *PTEN* 3′UTR (Figure S1B) and demonstrated via real-time PCR analysis that the *PTEN* 3′UTR RIP in DU145 prostate cancer cells significantly enriched for miR-17-5p, 19a, 19b, 20a, 26a, 93, 106a, and 106b compared to empty vector and IgG controls and a nontargeting microRNA control (miR-191) (Figure 1B). These results further support the claim that these microRNAs, which were previously validated mainly by overexpression and/or knockdown experiments, are bona fide *PTEN*-targeting microRNAs in this cell line and justify their inclusion in our analyses.

We next used the rna22 microRNA target prediction algorithm (Miranda et al., 2006) available at http://cbcsrv.watson.ibm.com/rna22.html to generate MuTaME scores for the entire human protein-coding transcriptome. The choice of rna22 was based on earlier reports supporting its low rate of false prediction (Hammell et al., 2008; Ritchie et al., 2009). A central tenet of our hypothesis is that *trans*-regulatory ceRNA crosstalk increases with the number of microRNAs that are shared by transcripts. This is the first consideration in deriving a MuTaMe score. The second consideration results from an often ignored dependence on the length of the candidate transcript's 3′UTR: the expected number of spurious microRNA target predictions increases with the length of the candidate 3′UTR through a nonlinear relationship (Altschul et al., 1990; Miranda et al., 2006), and this holds true independently of the algorithm used to predict microRNA targets. This dependence on length and the findings described in Miranda et al. and Ritchie et al. (Miranda et al., 2006; Ritchie et al., 2009) suggest that scenarios in which (1) there are many predicted MREs in a candidate transcript, (2) the MREs are spread over a relatively short span and are as evenly distributed within the span as possible, and (3) multiple MREs are predicted for each of the microRNAs under consideration ought to be favored.

To summarize, MuTaME evaluates a candidate ceRNA *X* based on the following: (1) how many microRNAs it shares with the mRNA *M* of interest. In our case, this is *PTEN* and is captured by the ratio of *#microRNAs predicted to target X* over *#microRNAs being considered*, which increases with the number of targeting microRNAs that *X* shares with *M*; (2) the number of MREs predicted in *X* for the *i*-th microRNA and the width of the span that they cover. This is captured by the ratio of *#MREs in X for i-th microRNA* over *distance between leftmost and rightmost predicted MRE for the i-th microRNA*, which favors situations in which more MREs spanning shorter distances are predicted for the *i*-th microRNA, and it captures one of the main observations in (Ritchie et al., 2009); (3) how evenly distributed the predicted MREs for the *i*-th microRNA are over the distance they span in *X*. This is captured by the ratio of *square of the distance between leftmost and rightmost predicted MRE for the i-th microRNA* over *sum of the squared distances between successive MREs of the i-th microRNA*, which favors more evenly distributed MREs for each microRNA and penalizes cases in which the majority, but not all, of a microRNA's MREs aggregate in a narrow neighborhood; and (4) the relation between the total number of MREs predicted in X compared to the total number of microRNAs that give rise to these MREs. This is captured by the ratio of (*#MREs in X for all considered microRNAs* − *#microRNAs predicted to target X + 1*) over *#MREs in X for all considered microRNAs*, which favors situations in which each targeting microRNA gives rise to more than one MRE in *X*. A priori, there is no reason to favor one type of contribution more than the rest, and thus, each candidate transcript *X* receives a combined MuTaMe score obtained simply by multiplying these four components. Furthermore, for our specific setting, we set stringent criteria and required that (1) a candidate ceRNA be targeted by at least seven of the ten validated *PTEN*-targeting microRNAs and (2) all predicted MREs occur only in the candidate ceRNA's 3′UTR. One potential concern here is whether this scoring approach would be biased in favor of transcripts *X* with longer 3′UTRs. Notably, we observed no correlation between 3′UTR length and MuTaMe score (corr = −0.13) or between 3′UTR length and the number of microRNAs predicted to target a candidate ceRNA (corr = 0.07). Using MuTaMe, we identified 158 candidate protein-coding transcripts representing 136 distinct genes as putative *trans*-regulators of PTEN (Figures 1C and 1D and Table S1). Intriguingly, the candidates displayed a nonrandom enrichment in selected biological categories (Figure S1C).

Putative PTEN ceRNAs Are Coexpressed with PTEN In Vivo

As our hypothesis predicts that transcripts within a ceRNA network are coregulated, we first examined whether putative

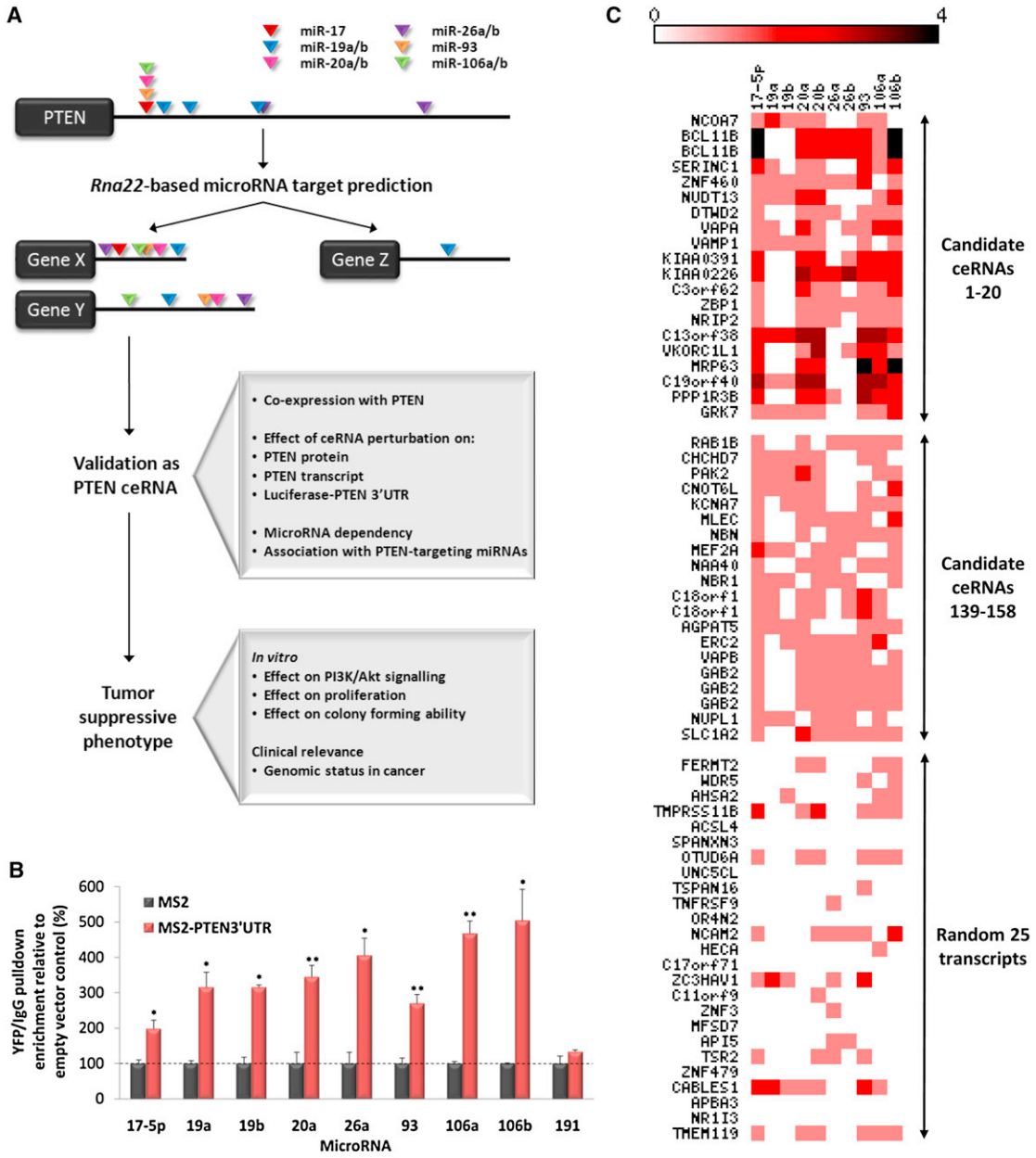

D

Predicted ceRNA rank	Gene	MuTaME score	17-5p	19a	19b	20a	20b	26a	26b	93	106a	106b	Total miRs	Total sites
-	PTEN	-	1	1	3	1	1	2	2	1	1	1	10	14
1	NCOA7	0.051	1	2	1	1	1	-	-	1	1	-	7	8
2	BCL11B	0.034	2	-	-	2	3	1	2	2	1	4	8	17
3	SERINC1	0.033	2	1	-	1	1	-	-	2	1	2	7	10
4	ZNF460	0.026	1	1	1	1	1	1	1	2	-	1	9	10
5	NUDT13	0.023	1	1	1	2	2	-	-	-	1	2	7	10
6	DTWD2	0.022	1	-	-	1	1	1	-	1	1	1	7	7
7	VAPA	0.018	1	1	-	2	1	-	1	1	2	2	8	11

Figure 1. Mutually Targeted MRE Enrichment Analysis Predicts Competitive Endogenous RNAs for PTEN

(A) Schematic outlining the mutually targeted MRE enrichment (MuTaME) analysis and subsequent experimental validation strategy. Validated PTEN-targeting microRNAs were used to predict putative PTEN ceRNAs. Candidates sharing at least seven microRNAs were considered putative PTEN ceRNAs.

PTEN ceRNAs are coexpressed with *PTEN* in human samples. We selected the top seven candidates from our MuTaME analysis (*NCOA7*, *BCL11B*, *SERINC1*, *ZNF460*, *NUDT13*, *DTWD2*, and *VAPA*) (Figure 1D) and investigated whether their expression correlated with *PTEN* expression in human prostate cancer (GSE21032) and glioblastoma (GSE15824), malignancies commonly defined by reduced PTEN levels. Significantly, *NCOA7*, *SERINC1*, *ZNF460*, and *VAPA* showed differential expression when samples were subdivided according to *PTEN* expression levels in both prostate cancer (179 total samples: 29 normal, 150 tumor) and glioblastoma (45 total samples: 5 normal, 40 tumor) (Figures 2A, 2B, and S2A). Expression of these four genes was also significantly correlated with PTEN transcript levels (Figure S2C).

As the prostate cancer study contained integrated expression profiling of both mRNAs and microRNAs, we were also able to rank patient samples according to microRNA expression levels. This enabled us to assess whether microRNA expression levels impact the coexpression correlation of PTEN ceRNAs and *PTEN*. Taking into account only the expression levels of the ten validated *PTEN*-targeting microRNAs used in our analysis, we subdivided samples into two groups: the first in which microRNAs were expressed at a lower level compared to their expression level in all samples and the second in which they were expressed at a higher level. The Pearson correlation coefficients between *PTEN* and its candidate ceRNAs were calculated in both groups, and intriguingly, we found an increase in correlation between *SERINC1*, *ZNF460*, and *VAPA* expression levels and *PTEN* when the microRNA expression was taken into consideration (Figure 2C). *NCOA7* was not significantly correlated with *PTEN* in this analysis (Figure S2B).

The significant correlation between *PTEN* expression and *SERINC1*, *ZNF460*, and *VAPA* expression and the sensitivity of this correlation to microRNA expression levels support our hypothesis that ceRNA transcripts can regulate *PTEN* levels in a biologically relevant manner. We next examined the coexpression of these three genes with *PTEN* in a database of multitissue and tissue-specific conserved human-mouse gene coexpression networks (Piro et al., 2011) and found that these genes were present in the top 1% of genes coexpressed with *PTEN* in several human-specific coexpression networks (Figure S2E). Based on their consistent coexpression with *PTEN*, we selected *SERINC1*, *ZNF460*, and *VAPA* for subsequent experimental validation.

Additionally, to investigate the extent to which lower-ranking candidates from our list exerted regulatory control over PTEN, we first explored the correlation of the 20 transcripts on our list with the lowest MuTaME scores with *PTEN* as described above. One of the most significantly correlated transcripts in both the prostate cancer and glioblastoma data sets was *CNOT6L*, which was also found to be significantly correlated with *PTEN* in the largest number of multitissue and tissue-specific conserved human-mouse gene coexpression networks (Figure S2D). We thus selected it as another candidate for further validation analysis.

PTEN ceRNAs Modulate PTEN Levels

We investigated the ability of these putative PTEN ceRNAs to modulate PTEN levels by first examining the effect of depletion of these candidates on endogenous PTEN protein levels in DU145 prostate cancer cells (Figure 3A). For this analysis, we also included two genes, *ACSL4* and *UNC5CL*, which are not predicted targets of these *PTEN*-targeting microRNAs as negative controls (Figure 1C). These experiments were performed using siRNA pools (a combination of four independent siRNAs), which are designed to achieve strong on-target gene knockdown with minimal off-target effects. Real-time PCR analysis confirmed efficient siRNA-mediated knockdown of candidate PTEN ceRNAs (Figure S3A). Depletion of *SERINC1*, *ZNF460*, *VAPA*, or *CNOT6L* transcripts did indeed result in a significant reduction in PTEN protein levels, whereas depletion of *ACSL4* or *UNC5CL* did not have a significant effect (Figures 3A and 3B). Moreover, reduced PTEN protein levels were accompanied by a concomitant, albeit less significant, decrease in *PTEN* transcript levels for *SERINC1*, *VAPA*, and *CNOT6L* knockdown (Figure 3B).

To ascertain whether this observed effect is dependent upon regulation of the *PTEN* 3′UTR, we constructed a chimeric luciferase construct tagged with the *PTEN* 3′UTR (Luc-PTEN3′UTR). This approach allows us to uncouple regulation of PTEN via 3′UTR-targeting microRNAs from *PTEN* mRNA transcription and protein stability. siRNA-mediated reduction of *SERINC1*, *VAPA*, and *CNOT6L* transcripts in Luc-PTEN3′UTR-expressing cells significantly lowered luciferase activity (Figure 3C). However, siRNA-mediated *ZNF460* knockdown did not significantly reduce Luc-PTEN3′UTR activity, suggesting that the observed effect on PTEN protein is not solely mediated by the *PTEN* 3′UTR. We thus excluded it from subsequent analysis.

Conversely, ectopic overexpression of *PTEN* ceRNA 3′UTRs in DU145 cells led to a marked upregulation of both Luc-PTEN3′UTR and endogenous protein levels, similar to the effect of overexpression of the PTEN 3′UTR on PTEN protein levels (Figures 3D–3F). Due to their large size, the *VAPA* and *CNOT6L* 3′UTRs were each cloned as two separate fragments subdivided based on the location of predicted MREs. Thus, sequestration of only a fraction of *PTEN*-targeting microRNAs may impact PTEN expression.

MicroRNA Dependency of ceRNA-Mediated PTEN Regulation

To investigate the microRNA dependency of ceRNA-mediated PTEN regulation, we utilized isogenic wild-type and DICER mutant HCT116 colon carcinoma cells. In the latter, gene targeting was used to disrupt a well-conserved segment of the N-terminal helicase domain in exon 5 of DICER (Cummins et al., 2006). As DICER is a critical enzyme involved in the

(B) MS2-RIP followed by microRNA RT-PCR to detect microRNAs endogenously associated with PTEN 3′UTR. Mean ± SD; $n \geq 3$; *$p < 0.05$; **$p < 0.01$.
(C) Heat map showing MRE enrichment of the top 20 (top) and bottom 20 (middle) putative PTEN ceRNAs and 25 randomly selected transcripts (bottom).
(D) Table summarizing predicted MREs in the 3′UTRs of the top seven putative PTEN ceRNAs.
See also Figure S1 and Table S1.

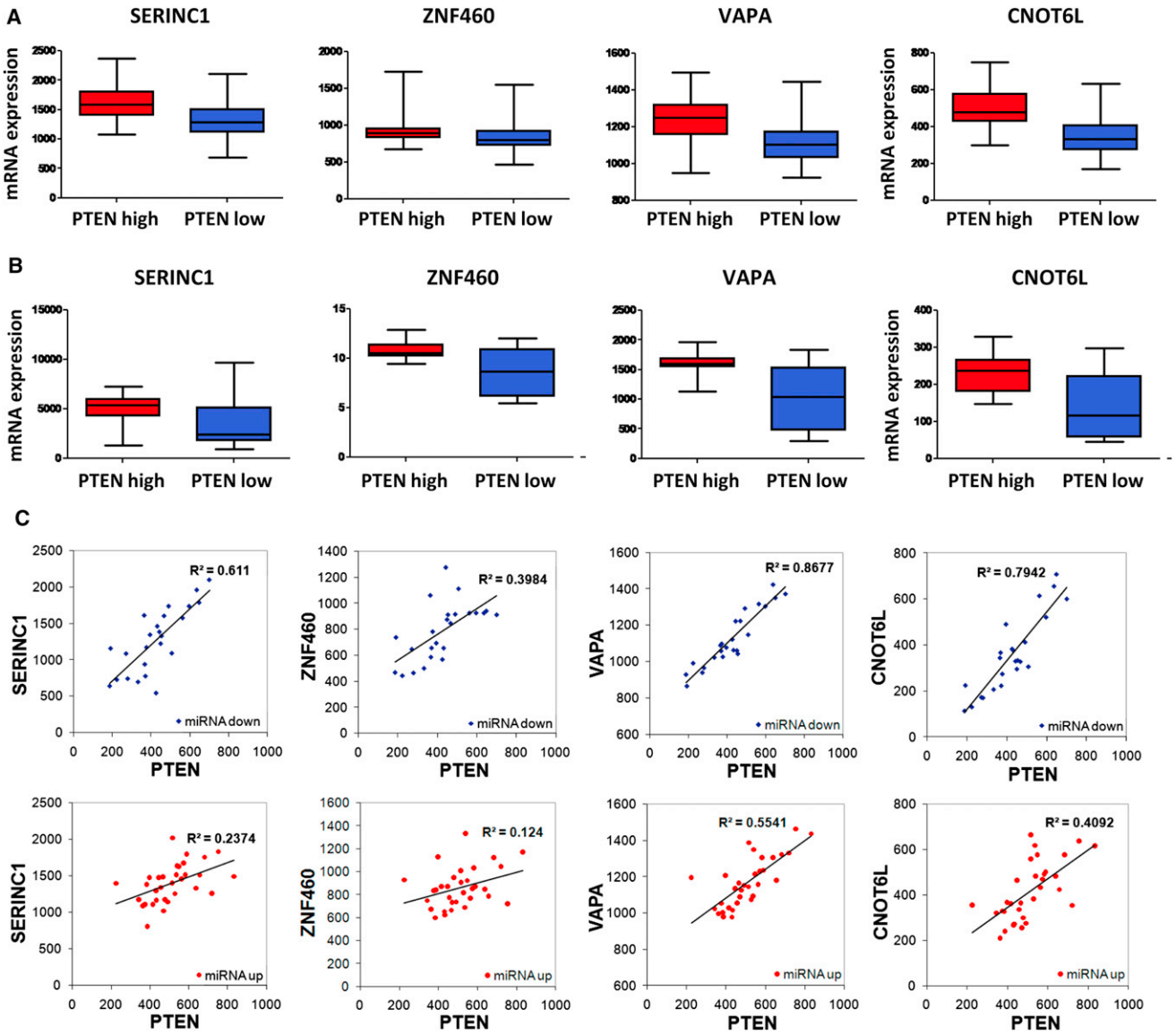

Figure 2. Coexpression of PTEN and PTEN ceRNAs in Human Cancer

(A and B) Comparison of PTEN ceRNA expression levels in primary (A) prostate cancer and (B) glioblastoma between two subsets of samples: "PTEN high" and "PTEN low," classified according to the average PTEN expression level. $p < 0.001$ except for SERINC1 in glioblastoma, in which $p = 0.009$. The ends of the whiskers represent the minimum and maximum of all the data.

(C) Coexpression analysis of PTEN and PTEN ceRNAs in subsets of the human prostate cancer specimens analyzed in (A) with decreased (blue, top) or increased (red, bottom) expression of PTEN-targeting microRNAs. $p < 0.001$ for all graphs except for SERINC1 microRNA up ($p = 0.002$) and ZNF460 microRNA up ($p = 0.024$). See also Figure S2.

processing of mature microRNAs, the DICER^{Ex5} mutant cells presented an ideal system to evaluate microRNA-dependent effects. Though DICER processes the vast majority of mature microRNAs, not all microRNAs exhibit DICER-dependent processing. We thus assessed whether processing of the microRNAs used in our analyses (Figures 1A and 1B) is abrogated in DICER^{Ex5} HCT116 cells. Indeed, microRNA real-time PCR analysis confirmed that these microRNAs were significantly downregulated in DICER^{Ex5} HCT116 cells (Figure S3C). We also confirmed that siRNA-mediated gene silencing is independent of DICER processing and hence is fully functional in DICER^{Ex5} HCT116 cells (Figure S3B).

Similar to the experiments in DU145 prostate cancer cells, siRNA-mediated depletion of *SERINC1*, *VAPA*, or *CNOT6L* expression resulted in a significant downregulation of PTEN protein in wild-type HCT116 colon cancer cells (Figures 3G and 3H). Importantly, PTEN downregulation by ceRNA loss was profoundly attenuated in DICER^{Ex5} HCT116 cells (Figures 3G and 3H), suggesting that mature microRNAs are essential for the regulation of PTEN by these three transcripts.

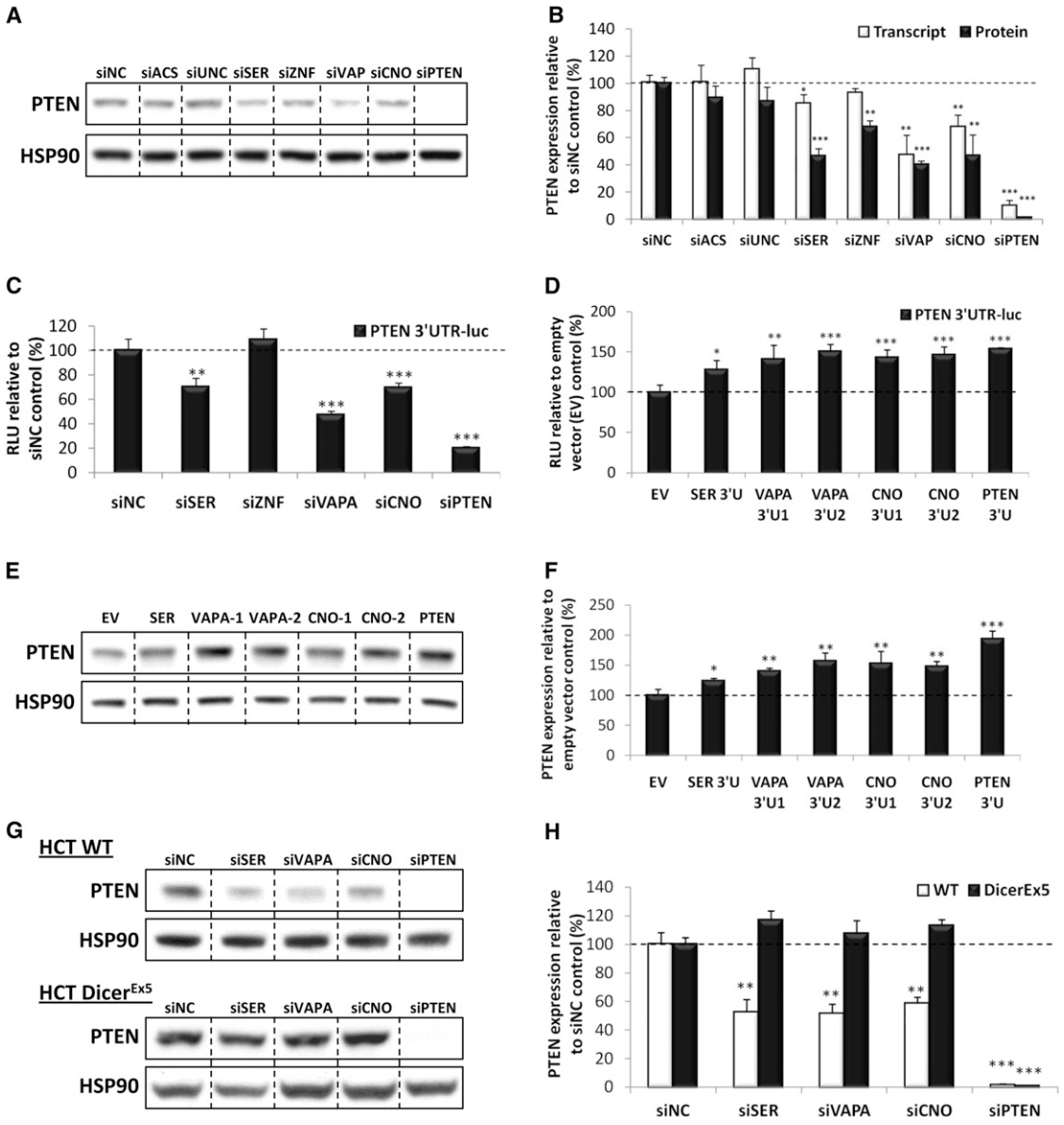

Figure 3. Putative PTEN ceRNAs Modulate PTEN Expression

(A) Western blot for PTEN protein levels in DU145 cells transfected with siRNA against predicted ceRNAs SERINC1 (siSER), ZNF460 (siZNF), VAPA (siVAPA), and CNOT6L (siCNO) and selected nontargeting controls ACSL4 (siACS) and UNC5CL (siUNC).

(B) Quantitation of PTEN protein shown in (A) and PTEN mRNA changes after transfection with siRNA against ceRNA as measured by RT-PCR.

(C) Luciferase activity in DU145 cells cotransfected with siRNA against PTEN ceRNAs and a luciferase-PTEN 3′UTR reporter construct.

(D) Luciferase activity in DU145 cells cotransfected with PTEN ceRNAs 3′UTRs and a luciferase-PTEN 3′UTR reporter construct.

(E) Western blot showing PTEN protein in response to overexpression of ceRNA 3′UTRs in DU145 cells.

(F) Quantitation of PTEN protein shown in (E).

(G) Western blot for PTEN in HCT116 WT (top) and *DICER*^{Ex5} (bottom) cells transfected with siRNAs against PTEN ceRNAs.

(H) Quantitation of PTEN protein shown in (G).

(B, D–F, and H) Mean ± SD; n ≥ 4; *p < 0.05; **p < 0.01; ***p < 0.001. See also Figure S3.

PTEN ceRNAs Are Regulated by PTEN-Targeting MicroRNAs

After successfully validating *SERINC1*, *VAPA*, and *CNOT6L* as bona fide PTEN ceRNAs that regulate PTEN levels in a microRNA-dependent manner, we next investigated their association with the *PTEN*-targeting microRNAs used in our analysis. We focused on VAPA and CNOT6L, as they had the most significant effect on PTEN at the 3′UTR level (Figures 3C–3F).

We constructed chimeric luciferase constructs tagged with the respective ceRNA 3′UTR fragments. As mentioned previously,

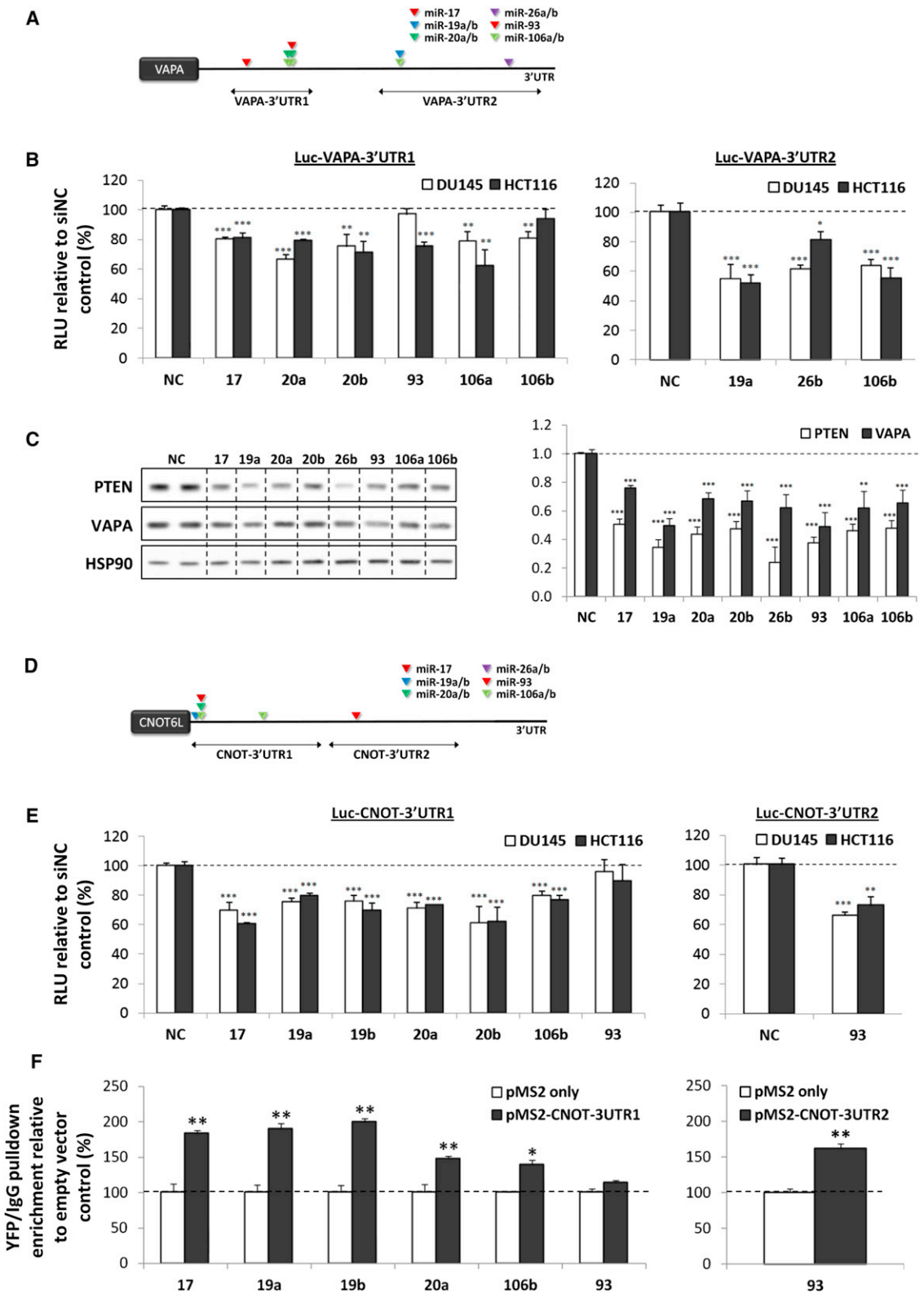

Figure 4. MicroRNA Dependency of PTEN ceRNA Function

(A) Schematic outlining the predicted binding sites of PTEN-targeting microRNAs to the 3′UTR of VAPA. The two fragments VAPA 3′UTR1 and VAPA 3′UTR2 were used for the luciferase experiments.

the *VAPA* and *CNOT6L* 3′UTRs were each cloned as two separate fragments subdivided based on the location of predicted MREs due to their large size (Figures 4A and 4D). Expression of miR-17, 20a, 20b, and 106a significantly reduced Luc-VAPA-3′UTR1 activity, and expression of miR-19a, 26b, and 106b significantly reduced Luc-VAPA-3′UTR2 activity in both DU145 and wild-type HCT116 cells (Figure 4B). The effect of miR-93 and 106b appeared to be cell type specific: miR-93 significantly reduced Luc-VAPA-3′UTR1 activity in HCT116 wild-type cells only, whereas miR-106b significantly reduced Luc-VAPA-3′UTR1 activity in DU145 cells only (Figure 4B).

Consistent with the luciferase results, overexpression of miRs 17, 19a, 20a, 20b, 26b, 106a, and 106b caused a significant downregulation of VAPA protein levels (Figure 4C). These results confirm that these validated PTEN-targeting microRNAs also regulate VAPA protein levels via its 3′UTR. Overexpression of miR-93 also resulted in a significant reduction of VAPA protein levels, in contrast to its effect on the Luc-VAPA-3′UTR1 reporter. This suggests that miR-93 is able to regulate VAPA protein levels independently of its 3′UTR, perhaps via targeting MREs located outside of the 3′UTR or modulation of upstream regulators. It is important to note that the effects of the various microRNAs on VAPA were consistently less profound than on those on PTEN. This result is in agreement with the fact that VAPA transcript is expressed at levels significantly higher than *PTEN* in DU145 cells (100-fold), a factor that may significantly increase its efficacy as a PTEN ceRNA (Figure S4A).

As predicted, miR-17, 19a, 19b, 20a, 20b, and 106b significantly reduced Luc-CNO-3′UTR1 activity in both DU145 and wild-type HCT116 cells (Figure 4E). Transfection of miR-93 significantly reduced the activity of Luc-CNO-3′UTR2, but not Luc-CNO-3′UTR1, consistent with the location of the predicted MRE (Figure 4E). As we were unable to find a good antibody for CNOT6L for western blot analysis, we instead performed RIP to confirm the physical association of these microRNAs with the *CNOT6L* 3′UTR. RIP for *CNOT6L* 3′UTR1 in DU145 prostate cancer cells significantly enriched for miR-17-5p, 19a, 19b, 20a, and 106b compared to empty vector and IgG controls, whereas RIP for *CNOT6L* 3′UTR2 significantly enriched for only miR-93 (Figure 4F). Expression of miR-20b was not detected, possibly due to its low level of endogenous expression (Figure S1A). These results therefore confirm the microRNA:3′UTR associations predicted by our MuTaME analysis.

Reciprocal ceRNA Interactions

Furthermore, we postulate that ceRNA networks will behave in a mutually reciprocal manner, i.e., ceRNAs will regulate one another bidirectionally. In an effort to study the network and reciprocal effects of ceRNA misexpression, we investigated the ability of PTEN downregulation to modulate VAPA protein expression and vice versa. We could not perform this experiment for CNOT6L due to the lack of specific antibodies, as mentioned above. Interestingly, we observed that siRNA knockdown of PTEN was able to significantly reduce VAPA expression in both DU145 and HCT116 cells (Figure S4B, top and middle), thus identifying regulatory loops between ceRNAs. This reciprocal regulation was at least partially microRNA dependent, as it was significantly lost in DICER^{Ex5} HCT116 cells (Figure S4B, bottom).

Attenuated Expression of PTEN ceRNAs Activates the PI3K/AKT Pathway

We next investigated the biological function of CNOT6L and VAPA in accordance with defined experimental criteria (Figure 1A). On the basis of our hypothesis, the net output of any given gene on oncogenic PI3K/AKT signaling encompasses their protein function, as well as ceRNA effect on PTEN and other transcripts. We therefore decided to determine which of the PTEN ceRNAs would not solely regulate PTEN, but also yield a robust suppressive effect on PI3K/AKT as well as on growth- and tumor-promoting activities. First, we evaluated the consequences of ceRNA-mediated PTEN regulation on the activation of the PI3K pathway. Aberrant activation of the PI3K/AKT pathway, at least in part, accounts for the protumorigenic effect of PTEN loss. DU145 cells depleted of individual PTEN ceRNAs were serum starved and restimulated, and AKT activation was determined. Consistent with the effect on PTEN protein levels, abrogation of CNOT6L or VAPA expression significantly elevated phospho-Akt (p-Akt) levels in response to serum stimulation (Figure 5A).

Depletion of CNOT6L in wild-type HCT116 augmented AKT activation in response to serum starvation and restimulation (1.6- and 2.1-fold change at 5 and 15 min, respectively, relative to the negative control transfection at the same time points) (Figure 5A), similar to the effects observed in DU145 cells. Similarly, VAPA depletion elevated p-Akt levels postrestimulation (1.8- and 2.1-fold change at 0 and 5 min, respectively, relative to the negative control transfection at the same time points) (Figure 5A). Notably, the effect of CNOT6L depletion on p-AKT was completely abrogated in DICER^{Ex5} HCT116 cells (p-Akt levels at 5 and 15 min were 0.9- and 0.4-fold, respectively, relative to the negative control transfection at the same time points), and the effect of VAPA depletion was significantly reduced (p-Akt levels at 0 and 5 min were 0.8- and 1.4-fold, respectively, relative to the negative control transfection at the same time points) (Figure 5A). Our results therefore demonstrate that downregulation of CNOT6L and VAPA activated the PI3K/AKT pathway in

(B) Luciferase activity in DU145 cells cotransfected with validated PTEN-targeting microRNAs predicted to target VAPA and luciferase-VAPA-3′UTR1 and 3′UTR2 reporter constructs.

(C) Western blot analysis of PTEN and VAPA expression in DU145 cells transfected with validated PTEN-targeting microRNAs predicted to target VAPA.

(D) Schematic outlining the predicted binding sites of PTEN-targeting microRNAs to the 3′UTR of CNOT6L. The two fragments CNOT 3′UTR1 and CNOT 3′UTR2 were used for the luciferase and RIP experiments.

(E) Luciferase activity in DU145 cells cotransfected with validated PTEN-targeting microRNAs predicted to target CNOT6L and luciferase-CNOT-3′UTR1 and 3′UTR2 reporter constructs.

(F) RIP followed by microRNA RT-PCR shows enrichment of PTEN-targeting microRNAs associated with CNOT6L 3′UTR.

(B, C, E, and F) Mean ± SD; $n \geq 4$; *$p < 0.05$; **$p < 0.01$; ***$p < 0.001$. See also Figure S4.

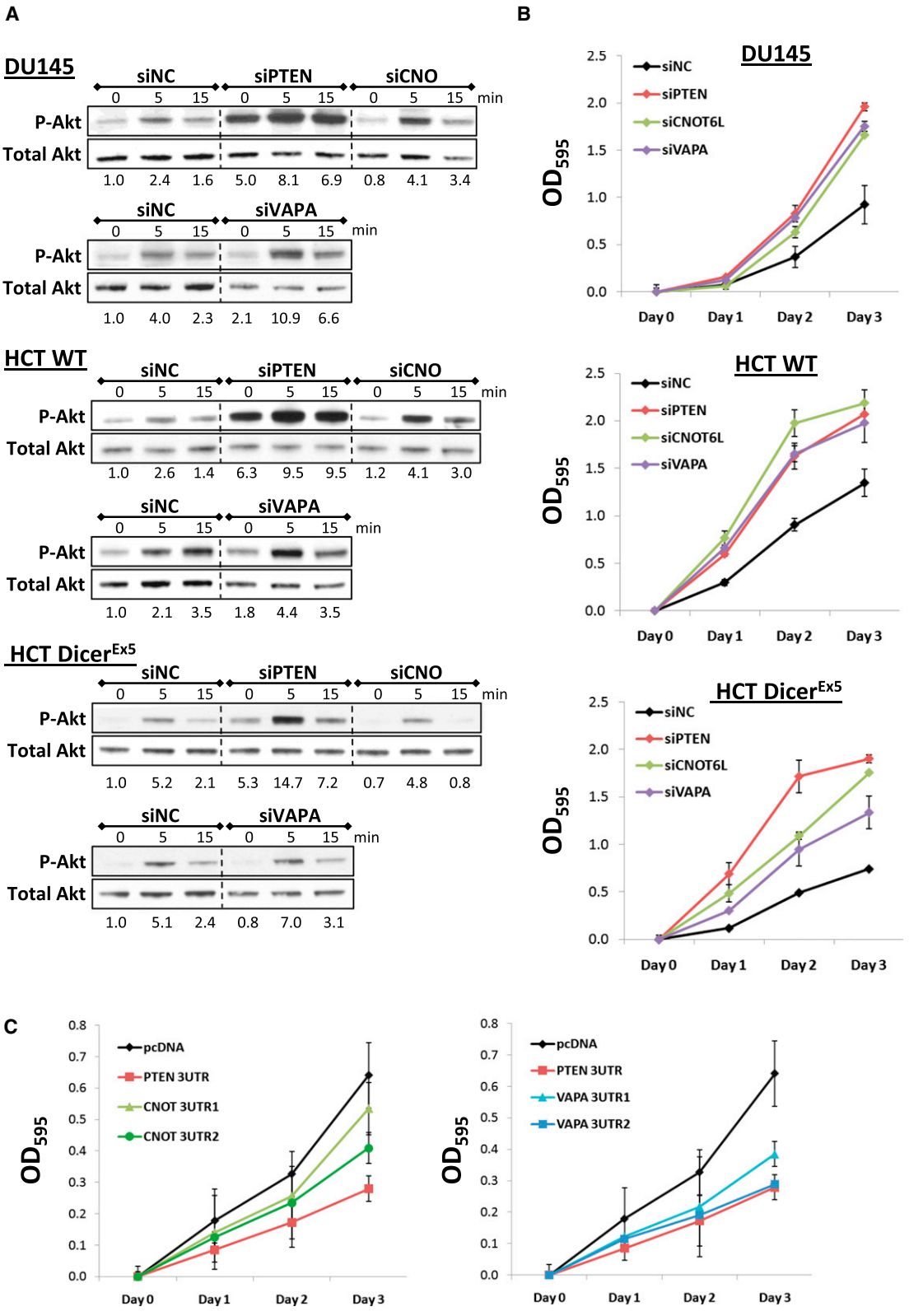

Figure 5. Depletion of PTEN ceRNAs Activates the PI3K/AKT Pathway and Promotes Growth In Vitro

(A) Western blot for phospho-AKT following serum starvation and restimulation of PTEN ceRNA siRNA-transfected DU145 cells (top), HCT116 WT (middle), and *DICER*$^{-/-}$ cells (bottom). Quantitation of western analyses is shown below the respective blots.

a microRNA-dependent manner, consistent with their role as PTEN ceRNAs.

PTEN ceRNAs Display Tumor-Suppressive Properties

As CNOT6L and VAPA appeared to phenocopy PTEN loss-mediated AKT activation based on their function as PTEN ceRNAs, we next determined whether these ceRNAs possess tumor-suppressive properties, as well as their status in human cancer (Figure 1A). To address this, we first evaluated cell proliferation and transformation in response to siRNA-mediated silencing of these PTEN ceRNAs. Reduced expression of CNOT6L or VAPA in cell lines where PTEN is regulated by these ceRNAs (DU145 and HCT116) resulted in a significant increase in proliferation similar to that observed with the PTEN siRNA (Figure 5B, top and middle). This effect on growth was significantly attenuated in the DICER^{Ex5} cells, suggesting that it is partially microRNA dependent (Figure 5B, bottom). Conversely, ectopic overexpression of 3′UTRs from *PTEN* and its ceRNAs, *CNOT6L* or *VAPA*, in DU145 cells led to a significant reduction in proliferation, suggesting that the observed phenotype is at least partially coding independent (Figure 5C). Moreover, depletion of CNOT6L or VAPA in DU145 cells promoted anchorage-independent growth in semisolid medium (Figure 6A).

Further support for the tumor-suppressive function of CNOT6L is provided in a Sleeping Beauty insertional mutagenesis screen in oncogenic BRAF-induced melanoma, which reports that *CNOT6L*, along with other PTEN ceRNAs, are subjected to a significant enrichment of transposon insertion sites (Karreth et al., 2011 [this issue of *Cell*]). *PTEN* itself was one of the most significant targets of insertion discovered in this study, validating the ability of this approach to identify genes implicated in human melanoma. Thus, *CNOT6L* dysregulation may be relevant for cancer development in an in vivo mouse model.

Finally, we examined alterations of the *CNOT6L* and *VAPA* genomic loci in human cancer. Remarkably, in a large data set of colon cancer (GSE11417, normal n = 56, colon adenocarcinoma n = 52) (Kurashina et al., 2008), copy number loss of both *CNOT6L* ($p = 3.19e^{-6}$, t test = −4.926) and *VAPA* ($p = 1.37e^{-7}$, t test = −5.834) was present in a significant population of samples (Figure 6B). *PTEN* was also significantly downregulated in this data set ($p = 1.74e^{-4}$, t test = −3.810). These data demonstrate the existence of significant copy number losses at both the *VAPA* and *CNOT6L* genomic loci, supporting the hypothesis that they possess tumor-suppressive properties and are under selective pressure to undergo copy number losses in cancer.

DISCUSSION

The findings presented herein have allowed us to reach a number of important conclusions. First, we demonstrate that protein-coding mRNA transcripts can crosstalk with other mRNA transcripts by competing for common microRNAs, hence attributing to protein-coding mRNA transcripts a previously unrecognized noncoding function that is encrypted in the mRNA itself. Second, we establish that this crosstalk occurs through a language based on MREs that allows for bioinformatic predictions toward the definition of the ceRNA network for a given mRNA. An important implication of our findings is that, in addition to their function as *cis* regulatory elements that regulate the expression of their own transcripts, 3′UTRs are also *trans* modulators of gene expression through microRNA binding. This is particularly important given the identification of 3′UTRs expressed separately from the associated protein-coding sequences to which they are normally linked (Mercer et al., 2011).

Third, we propose a set of defined rules and have developed a methodology to identify, classify, and validate protein-coding ceRNAs that can crosstalk by identifying shared MREs. We have demonstrated that our approach can be predictive in finding ceRNAs that can modulate PTEN through microRNA competition. More generally, in doing so, we have identified a unique means to rapidly identify previously uncharacterized mRNA regulators.

Moreover, our MRE matching methodology has allowed us to identify ceRNAs with putative tumor-suppressive function, which is exerted, at least in part, through their ability to modulate PTEN and the PI3K signaling output (Figure 6C). This, in turn, functionally links a number of unexpected biological and tumor-suppressive pathways to the proto-oncogenic PTEN/PI3K-signaling pathway through the ceRNA noncoding language (Figure S1C). For example, CNOT6L is a cytoplasmic deadenylase that is involved in poly(A) tail shortening (Wang et al., 2010), and vesicle-associated membrane protein-associated protein-A (VAPA) is an integral membrane protein implicated in transport between the endoplasmic reticulum and Golgi vesicle (Prosser et al., 2008; Wyles et al., 2002).

These ceRNAs were not functionally linked to PTEN before and have been now related to this critical tumor suppressor on the sole basis of their predicted ceRNA function. We have validated this interaction by measuring the coexpression of such ceRNAs with PTEN, determining the growth/tumor-suppressive function of such ceRNAs, and demonstrating that the expression of these ceRNAs and their allelic status is decreased in cancer specimens as determined by interrogating large cancer-derived gene expression data sets. Further validation stems from our identification of PTEN ceRNAs, including CNOT6L, in vivo in an oncogenic BRAF-induced mouse model of melanoma (Karreth et al., 2011 [this issue of *Cell*]).

We had recently proposed that the ceRNA language would allow RNA to communicate (Salmena et al., 2011). However, it remained to be established whether this theory could be translated into useful predictions. In this study, we define a comprehensive and integrated bioinformatic and experimental

(B) Proliferation curve of DU145 cells (top), HCT116 WT (middle), and *DICER*$^{-/-}$ cells (bottom) transfected with siRNAs against PTEN ceRNAs. siPTEN, siCNOT6L, and siVAPA result in a significant increase in growth relative to the siNC control in DU145 and HCT WT cells ($p < 0.001$ in DU145; $p < 0.01$ in HCT WT). In the *HCT D*$^{-/-}$ cells, siCNOT6L ($p < 0.05$) and siVAPA ($p < 0.01$) result in a significant decrease in growth relative to the siPTEN positive control.

(C) Proliferation curve of DU145 cells transfected with plasmids overexpressing PTEN or ceRNA 3′UTRs. Relative to the empty vector control (pcDNA) transfection, CNOT 3′UTR2 ($p < 0.05$), VAPA 3′UTR1 ($p < 0.05$), VAPA 3′UTR2 ($p < 0.001$), and PTEN 3′UTR ($p < 0.001$) result in a significant decrease in growth.

(B and C) Mean ± SD; $n \geq 3$.

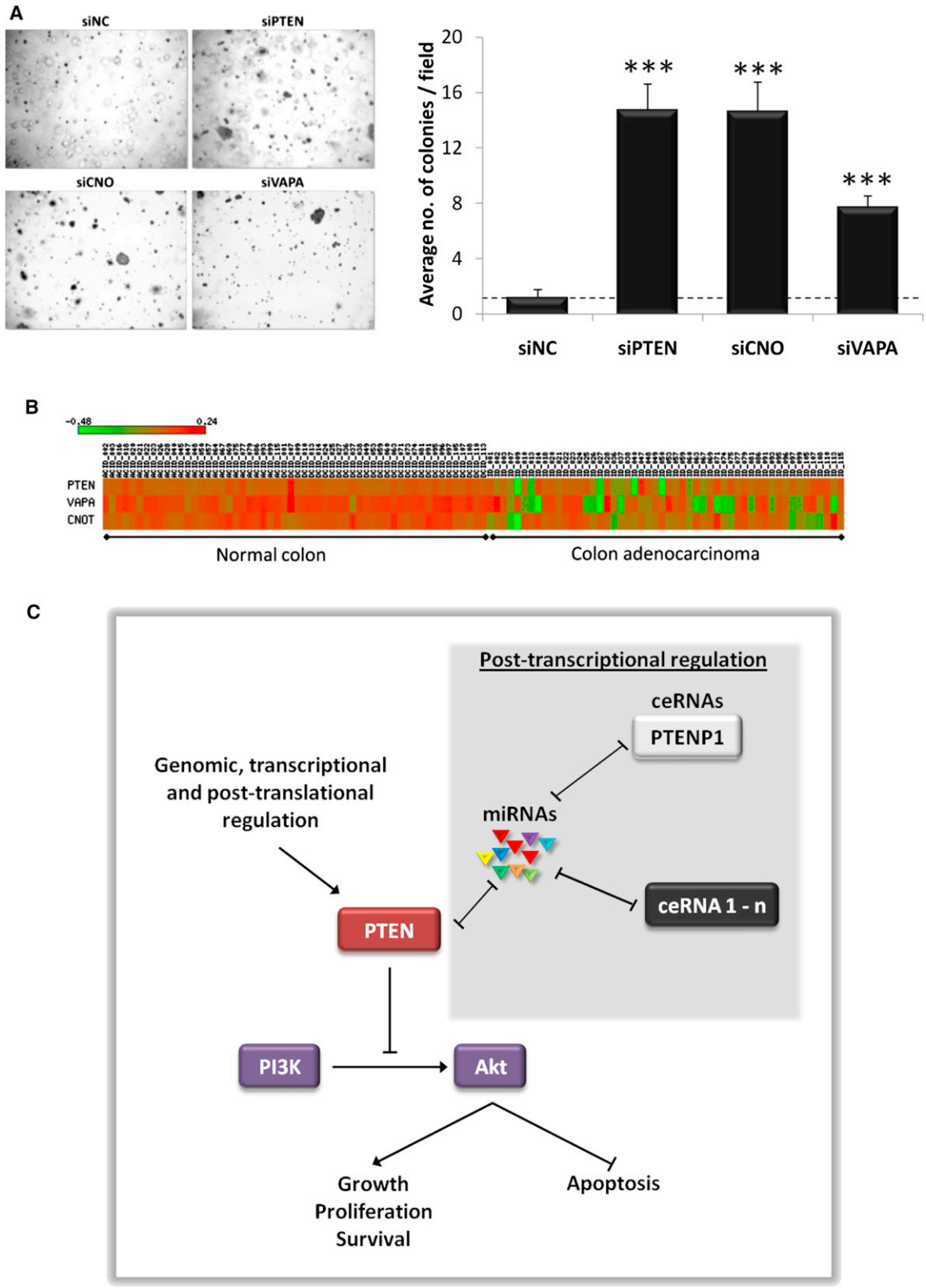

Figure 6. VAPA and CNOT6L Possess Tumor-Suppressive Properties

(A) Anchorage-independent growth of DU145 cells transfected with siRNAs against PTEN ceRNAs in semisolid medium. Bottom panel shows quantitation of colony formation after 10 days. Mean ± SE; n ≥ 3; ***p < 0.001.

approach for the prediction and validation of ceRNA activity and networks. This approach can therefore be employed to identify and validate ceRNAs for other mRNAs of interest. That the identification of ceRNAs is indeed possible through bioinformatic predictions is corroborated by an accompanying study (Sumazin et al., 2011 [this issue of *Cell*]). It is important to note that previous studies have reported a *trans*-regulatory modulation of gene expression through the binding of shared microRNAs, but these studies focused mainly on the regulation of a single microRNA (Cazalla et al., 2010; Lee et al., 2009) and of conserved ceRNAs such as pseudogenes (Poliseno et., 2010b). This study now extends this mechanism to potentially any mRNAs that share MREs and thus suggests the presence of a large regulatory network built from this extensive crosstalk among mRNAs.

Although we have focused only on protein-coding RNA, the fact that ceRNA function does not rely on the protein-encoding genetic blueprint that mRNA harbors within its nucleotide sequence suggests that all MRE-containing components of the transcriptome, including mRNAs, transcribed pseudogenes, and long noncoding RNAs (lncRNA), are capable of regulating each other in this manner. This is supported by an accompanying study in which the long noncoding RNA linc-MD1 is shown to regulate muscle differentiation by acting as a ceRNA for muscle differentiation factors MEF2C and MAML1 (Cesana et al., 2011, [this issue of *Cell*]).

We therefore propose that the ceRNA language expands the total collection of functional genetic information in our genome by orders of magnitude and attributes a noncoding function to protein-coding transcripts, which may play an important role in physiological processes and pathological conditions (Salmena et al., 2011). In this study, we have therefore identified an unanticipated dimension by which RNA molecules can communicate and exert their functions and a means to predict these functions through the annotation of the ceRNA language.

EXPERIMENTAL PROCEDURES

MicroRNA Target Prediction

MicroRNA target prediction was performed using Rna22, which is available through a graphical user interface or a batch utility at http://cbcsrv.watson.ibm.com/rna22.html (Miranda et al., 2006).

Reagents

Reagents are as follows: anti-HSP90 antibody 61041 (Becton Dickinson); anti-PTEN antibody 9559 (Cell Signaling); anti-VAPA antibody sc-98890 (Santa Cruz); siGENOME siRNA reagents for nontargeting 2 (siNC), PTEN (siPTEN), ZNF460 (siZNF), CNOT6L (siCNO), SERINC1 (siSER), VAPA (siVAPA), and Dharmafect 1 (Dharmacon); Lipofectamine 2000, Trizol reagent, Dulbecco's modified Eagle medium (DMEM), Opti-MEM reduced serum media, and fetal bovine serum (FBS) (Invitrogen); psiCHECK-2 vector and dual-luciferase reporter assay (Promega); and RNeasy mini kit, DNeasy blood and tissue kit, and Qiaprep spin miniprep kit (QIAGEN).

Plasmids

The 3′UTRs of PTEN, CNOT6L, SERINC1, and VAPA were amplified by PCR from the genomic DNA of DU145 cells and were cloned into pcDNA3.1+ according to standard protocols. Due to size constraints, CNOT6L and VAPA 3′UTRs were each cloned as two separate fragments. The PTEN 3′UTR was then subcloned into psiCHECK-2 using *XhoI* and *NotI* restriction sites. PTEN 3′UTR was also subcloned into the pMS2 vector for RIP analysis. Primer sequences are as follows: PTEN3′UTR-F TAGAGGAGCCGTCAAA TCCA, PTEN3′UTR-R CCCCCACTTTAGTGCACAGT, CNOT6L3′UTR1-F AA GACGGGGATCTGTTGCTA, CNOT6L3′UTR1-R GGGCTCCTCTGTGGTTC ATA, CNOT6L3′UTR2-F CCACCTACTGCTCCTTGCTC, CNOT6L3′UTR2-R CTTTTGCACGCACACTTTGT, SERINC13′UTR-F AGACTTCTAGCATGAAA GTCCCACT, SERINC13′UTR-R TTCATTTATTTAGAGGTAAAACACAGC, VAPA3′UTR1-F CCTTGTGAGGCAGTTGTTGA, VAPA3′UTR1-R TTTTGCA CACAAGCAAGAGG, VAPA3′UTR2-F TCACCTCACTGCAGCTTCC, and VAPA3′UTR2-R TGCAAAACTTTATTTTGATTCTCG.

Cell Culture and Transfection

DU145, HCT116 wild-type, and DICER^{Ex5} cells were grown in DMEM plus 10% FBS, penicillin/streptomycin, and glutamine at 37°C in a humidified atmosphere with 5% CO_2. For the transfection of siRNAs, DU145 or HCT116 were transfected with 100 nM siRNAs in 12-well dishes at a density of 100,000 or 130,000 cells per well, respectively. Transfection was performed with Dharmafect 1 according to the manufacturer's recommendations. With this protocol, more than 90% of cells were positive for the fluorescent siGLO RISC-free control siRNA (data not shown). For plasmid transfection, DU145 were seeded in 12-well dishes at a density of 120,000 cells per well. Transfection was performed 24 hr later with Lipofectamine 2000 according to the manufacturer's recommendations. Cells were trypsinized and seeded for the various assays 8 hr posttransfection.

Protein Extraction and Western Blot Analysis

Cells were washed in chilled PBS and lysed directly in the wells by incubating on ice for 20 min with RIPA lysis buffer containing protease inhibitors. Lysates were cleared by centrifugation at 4°C for 15 min at 12,100 × g, and protein concentrations were determined using Bradford dye (Bio-Rad). For western blot analysis, 10 μg of total protein was size fractionated by SDS-PAGE on 4%–12% Bis-Tris acrylamide NuPAGE gels in MOPS SDS running buffer (Invitrogen) and transferred to nitrocellulose membranes (Whatman) in NuPage transfer buffer (Invitrogen) containing 10% methanol. The membranes were then probed with specific primary antibodies (see "Reagents" in Experimental Procedures).

RNA Extraction and Real-Time PCR

For real-time PCR analyses, total RNA was extracted from cells using Trizol reagent as per the manufacturer's instructions and subsequently column purified with RNeasy kits (QIAGEN). cDNA synthesis was performed using the High Capacity cDNA Archive kit according to the manufacturer's instructions (Applied Biosystems). MicroRNA reverse transcription was performed with the microRNA reverse transcription kit according to manufacturer's instructions (Applied Biosystems). Real-time PCR was subsequently performed using the LightCycler 480 System (Roche Applied Science).

Luciferase Assays

MicroRNA target validation assays were performed as described previously (Tay et al., 2008). DU145 cells were seeded 24 hr before transfection at a density of 120,000 cells/well in 12-well plates. 100 ng of empty psiCHECK-2 vector or psiCHECK-2+PTEN3′UTR was cotransfected with 100nM siRNA or 1 μg vector constructs with Lipofectamine 2000 according to manufacturer's instructions. In all cases, a constitutively expressed firefly luciferase gene in psiCHECK-2 was used as a normalization control for transfection efficiency. At 72 hr after transfection, firefly and Renilla luciferase activities were measured consecutively with the dual-luciferase reporter system (Promega) using a luminometer (Promega).

(B) Heatmap depicting the genomic status of PTEN, VAPA, and CNOT6L in human colon adenocarcinoma compared to normal samples. Scale: $\log_2$ copy number units, p = $1.74e^{-4}$, $1.37e^{-7}$, and $3.19e^{-6}$ for PTEN, VAPA, and CNOT6L, respectively.
(C) Model of regulation of PTEN expression. Posttranscriptional regulation via sequestration of microRNAs by ceRNAs represents a *trans*-regulatory dimension of PTEN regulation.

Cell Proliferation

At 8 hr posttransfection, DU145 cells were trypsinized, resuspended, and seeded in four separate 12-well plates at a final density of 20,000/well. Starting from the following day (d0), one plate per day was washed once with PBS, fixed in 10% formalin solution for 10 min at room temperature, and then kept in PBS at 4°C. On the last day, all of the wells were stained with crystal violet. After lysis with 10% acetic acid, optical density was read at 595 nm.

Growth in Semisolid Medium

The bottom layer was obtained by covering 6-well dishes with 3 ml of 0.6% agar in DMEM. The day after, transfected DU145 cells were seeded on top in triplicate in 2 ml of 0.3% agar in DMEM plus 10% FBS. Colonies were counted after 10 days at 40× magnification.

RNA Immunoprecipitation and Analysis

Cells were lysed on ice 48 hr after transfection with MS2 plasmids (Kim et al., 2009), and RIPs were performed as previously described (Keene et al., 2006). Briefly, cell lysates were incubated overnight at 4°C with control Rabbit IgG (Jackson ImmunoResearch) or anti-YFP antibody (Santa Cruz) that were bound to Protein A Sepharose beads (Sigma). Beads were then washed five times with NT2 buffer, and RNA was eluted by incubation with SDS-TE buffer by heating at 55°C for 30 min. RNA was then precipitated using the standard Trizol (Invitrogen) protocol and analyzed via real-time PCR.

PTEN and ceRNA Coexpression Analysis and Genomic Status Assessment

Coexpression in prostate cancer was evaluated using GEO super-series GSE21032 (Taylor et al., 2010). From this data set, whole-transcript expression data for human primary and metastatic prostate cancer samples (GSE21034) and microRNA expression data for human primary and metastatic prostate cancer samples (GSE21036) were analyzed. Processed and normalized expression data were downloaded from NCBI. To study differential expression, samples were subdivided into two subsets according to PTEN expression: a PTEN-down subset with samples showing a PTEN expression level lower than the PTEN average value calculated among all samples and a PTEN-up subset characterized by a PTEN expression level higher than this average value. To select subsets of samples with lower or higher microRNA expression level, at least one microRNA out of ten microRNAs targeting PTEN was required to show an expression level lower (or higher) than a standard deviation from its average level; samples in which the different levels of expression among microRNAs were not consistent were discarded. Thirty-three samples were thus obtained for the subset with higher expression and 26 for that with lower expression. Differential expression in glioblastoma was assessed by the analysis of GEO series GSE15824. Processed and normalized expression data were downloaded from NCBI, and entrez gene ID were linked to Affymetrix probe sets by Affymetrix annotation na31. Coexpression between PTEN and the ceRNA genes were analyzed in multitissues, and normal tissue-specific human-mouse conserved and human-specific coexpression networks were generated from a specific annotated database (http://www.cbu.mbcunito.it/ts-coexp) (Piro et al., 2011); the coexpression was considered significant if it was found in the top 1% of the ranked list of genes coexpressed with PTEN. Genomic status was assessed using the GEO series GSE11417 (Kurashina et al., 2008). Oncomine (Compendia Bioscience, Ann Arbor, MI) was used for analysis and visualization (http://www.oncomine.org).

Statistical Analysis

In vitro data were analyzed using unpaired Student's t test. Values of $p < 0.05$ were considered statistically significant. *$p < 0.05$; **$p < 0.01$; ***$p < 0.001$. The mean ± SD of three or more independent experiments is reported.

SUPPLEMENTAL INFORMATION

Supplemental Information includes four figures and one table and can be found with this article online at doi:10.1016/j.cell.2011.09.029.

ACKNOWLEDGMENTS

We thank Pandolfi laboratory members for critical discussions. Real-time PCR analysis was conducted through the Harvard Catalyst Laboratory for Innovative Translational Technologies with support from Harvard Catalyst | The Harvard Clinical and Translational Science Center (NIH Award #UL1 RR 025758 and financial contributions from Harvard University and its affiliated academic health care centers). The content is solely the responsibility of the authors and does not necessarily represent the official views of Harvard Catalyst, Harvard University and its affiliated academic health care centers, the National Center for Research Resources, or the National Institutes of Health. We thank B. Vogelstein for DICER^{Ex5} cells, M. Gorospe for the pMS2 plasmids, and I. Legnini for experimental support. Y.T. was supported by a Special Fellow Award from The Leukemia & Lymphoma Society. L.K. was supported by an NHMRC Overseas Postdoctoral Fellowship. L.S. was supported by fellowships from the Human Frontier Science Program and the Canadian Institutes of Health Research. U.A. was supported by a fellowship from the Fondazione per la Ricerca Biomedica ONLUS of Torino. S.M.T. was supported by a Department of Defense (DOD) Breast Cancer Research Program (BCRP) postdoctoral fellowship award. P.P. and U.A. gratefully acknowledge support from the Italian Association for Cancer Research (AIRC) under grant IG-9408. I.R. was supported by funding from the Jefferson Medical College of Thomas Jefferson University. This work was supported, in part, by NIH grant R01 CA-82328-09 to P.P.P.

Received: August 11, 2011
Revised: September 17, 2011
Accepted: September 23, 2011
Published: October 13, 2011

REFERENCES

Alimonti, A., Carracedo, A., Clohessy, J.G., Trotman, L.C., Nardella, C., Egia, A., Salmena, L., Sampieri, K., Haveman, W.J., Brogi, E., et al. (2010). Subtle variations in Pten dose determine cancer susceptibility. Nat. Genet. *42*, 454–458.

Altschul, S.F., Gish, W., Miller, W., Myers, E.W., and Lipman, D.J. (1990). Basic local alignment search tool. J. Mol. Biol. *215*, 403–410.

Arvey, A., Larsson, E., Sander, C., Leslie, C.S., and Marks, D.S. (2010). Target mRNA abundance dilutes microRNA and siRNA activity. Mol. Syst. Biol. *6*, 363.

Bartel, D.P. (2009). MicroRNAs: target recognition and regulatory functions. Cell *136*, 215–233.

Bartel, D.P., and Chen, C.Z. (2004). Micromanagers of gene expression: the potentially widespread influence of metazoan microRNAs. Nat. Rev. Genet. *5*, 396–400.

Berger, A.H., Knudson, A.G., and Pandolfi, P.P. (2011). A continuum model for tumor suppression. Nature, in press.

Cazalla, D., Yario, T., and Steitz, J.A. (2010). Down-regulation of a host microRNA by a Herpesvirus saimiri noncoding RNA. Science *328*, 1563–1566.

Cesana, M., Cacchiarelli, D., Legnini, I., Santini, T., Sthandier, O., Chinappi, M., Tramontano, A., and Bozzoni, I. (2011). A long noncoding RNA controls muscle differentiation by functioning as a competing endogenous RNA. Cell *147*, this issue, 358–369.

Cummins, J.M., He, Y., Leary, R.J., Pagliarini, R., Diaz, L.A., Jr., Sjoblom, T., Barad, O., Bentwich, Z., Szafranska, A.E., Labourier, E., et al. (2006). The colorectal microRNAome. Proc. Natl. Acad. Sci. USA *103*, 3687–3692.

Friedman, R.C., Farh, K.K., Burge, C.B., and Bartel, D.P. (2009). Most mammalian mRNAs are conserved targets of microRNAs. Genome Res. *19*, 92–105.

Hammell, M., Long, D., Zhang, L., Lee, A., Carmack, C.S., Han, M., Ding, Y., and Ambros, V. (2008). mirWIP: microRNA target prediction based on microRNA-containing ribonucleoprotein-enriched transcripts. Nat. Methods *5*, 813–819.

Hollander, M.C., Blumenthal, G.M., and Dennis, P.A. (2011). PTEN loss in the continuum of common cancers, rare syndromes and mouse models. Nat. Rev. Cancer *11*, 289–301.

Huse, J.T., Brennan, C., Hambardzumyan, D., Wee, B., Pena, J., Rouhanifard, S.H., Sohn-Lee, C., le Sage, C., Agami, R., Tuschl, T., et al. (2009). The PTEN-regulating microRNA miR-26a is amplified in high-grade glioma and facilitates gliomagenesis in vivo. Genes Dev. *23*, 1327–1337.

Jeyapalan, Z., Deng, Z., Shatseva, T., Fang, L., He, C., and Yang, B.B. (2011). Expression of CD44 3′-untranslated region regulates endogenous microRNA functions in tumorigenesis and angiogenesis. Nucleic Acids Res. *39*, 3026–3041.

Karreth, F.A., Tay, Y., Perna, D., Ala, U., Tan, S.M., Rust, A.G., DeNicola, G., Webster, K.A., Weiss, D., Perez-Mancera, P.A., et al. (2011). In vivo identification of tumor-suppressive PTEN ceRNAs in an oncogenic BRAF-induced mouse model of melanoma. Cell *147*, this issue, 382–395.

Keene, J.D., Komisarow, J.M., and Friedersdorf, M.B. (2006). RIP-Chip: the isolation and identification of mRNAs, microRNAs and protein components of ribonucleoprotein complexes from cell extracts. Nat. Protoc. *1*, 302–307.

Kim, H.H., Kuwano, Y., Srikantan, S., Lee, E.K., Martindale, J.L., and Gorospe, M. (2009). HuR recruits let-7/RISC to repress c-Myc expression. Genes Dev. *23*, 1743–1748.

Kloc, M. (2008). Emerging novel functions of RNAs, and binary phenotype? Dev. Biol. *317*, 401–404.

Kurashina, K., Yamashita, Y., Ueno, T., Koinuma, K., Ohashi, J., Horie, H., Miyakura, Y., Hamada, T., Haruta, H., Hatanaka, H., et al. (2008). Chromosome copy number analysis in screening for prognosis-related genomic regions in colorectal carcinoma. Cancer Sci. *99*, 1835–1840.

Lee, D.Y., Shatseva, T., Jeyapalan, Z., Du, W.W., Deng, Z., and Yang, B.B. (2009). A 3′-untranslated region (3′UTR) induces organ adhesion by regulating miR-199a* functions. PLoS ONE *4*, e4527.

Mercer, T.R., Wilhelm, D., Dinger, M.E., Solda, G., Korbie, D.J., Glazov, E.A., Truong, V., Schwenke, M., Simons, C., Matthaei, K.I., et al. (2011). Expression of distinct RNAs from 3′ untranslated regions. Nucleic Acids Res. *39*, 2393–2403.

Miranda, K.C., Huynh, T., Tay, Y., Ang, Y.S., Tam, W.L., Thomson, A.M., Lim, B., and Rigoutsos, I. (2006). A pattern-based method for the identification of microRNA binding sites and their corresponding heteroduplexes. Cell *126*, 1203–1217.

Mu, P., Han, Y.C., Betel, D., Yao, E., Squatrito, M., Ogrodowski, P., de Stanchina, E., D'Andrea, A., Sander, C., and Ventura, A. (2009). Genetic dissection of the miR-17∼92 cluster of microRNAs in Myc-induced B-cell lymphomas. Genes Dev. *23*, 2806–2811.

Olive, V., Bennett, M.J., Walker, J.C., Ma, C., Jiang, I., Cordon-Cardo, C., Li, Q.J., Lowe, S.W., Hannon, G.J., and He, L. (2009). miR-19 is a key oncogenic component of mir-17-92. Genes Dev. *23*, 2839–2849.

Piro, R.M., Ala, U., Molineris, I., Grassi, E., Bracco, C., Perego, G.P., Provero, P., and Di Cunto, F. (2011). An atlas of tissue-specific conserved coexpression for functional annotation and disease gene prediction. Eur. J. Hum. Genet. Published online June 8, 2011. 10.1038/ehg.2011.96.

Poliseno, L., Salmena, L., Riccardi, L., Fornari, A., Song, M.S., Hobbs, R.M., Sportoletti, P., Varmeh, S., Egia, A., Fedele, G., et al. (2010a). Identification of the miR-106b∼25 microRNA cluster as a proto-oncogenic PTEN-targeting intron that cooperates with its host gene MCM7 in transformation. Sci. Signal. *3*, ra29.

Poliseno, L., Salmena, L., Zhang, J., Carver, B., Haveman, W.J., and Pandolfi, P.P. (2010b). A coding-independent function of gene and pseudogene mRNAs regulates tumour biology. Nature *465*, 1033–1038.

Prosser, D.C., Tran, D., Gougeon, P.Y., Verly, C., and Ngsee, J.K. (2008). FFAT rescues VAPA-mediated inhibition of ER-to-Golgi transport and VAPB-mediated ER aggregation. J. Cell Sci. *121*, 3052–3061.

Ritchie, W., Flamant, S., and Rasko, J.E. (2009). Predicting microRNA targets and functions: traps for the unwary. Nat. Methods *6*, 397–398.

Salmena, L., Poliseno, L., Tay, Y., Kats, L., and Pandolfi, P.P. (2011). A ceRNA hypothesis: the Rosetta Stone of a hidden RNA language? Cell *146*, 353–358.

Seitz, H. (2009). Redefining microRNA targets. Curr. Biol. *19*, 870–873.

Sumazin, P., Yang, X., Chiu, H.-S., Chung, W.-J., Iyer, A., Llobet-Navas, D., Rajbhandari, P., Bansal, M., Guarnieri, P., Silva, J., et al. (2011). An extensive microRNA-mediated network of RNA-RNA interactions regulates established oncogenic pathways in glioblastoma. Cell *147*, this issue, 370–381.

Tay, Y., Zhang, J., Thomson, A.M., Lim, B., and Rigoutsos, I. (2008). MicroRNAs to Nanog, Oct4 and Sox2 coding regions modulate embryonic stem cell differentiation. Nature *455*, 1124–1128.

Taylor, B.S., Schultz, N., Hieronymus, H., Gopalan, A., Xiao, Y., Carver, B.S., Arora, V.K., Kaushik, P., Cerami, E., Reva, B., et al. (2010). Integrative genomic profiling of human prostate cancer. Cancer Cell *18*, 11–22.

Trotman, L.C., Niki, M., Dotan, Z.A., Koutcher, J.A., Di Cristofano, A., Xiao, A., Khoo, A.S., Roy-Burman, P., Greenberg, N.M., Van Dyke, T., et al. (2003). Pten dose dictates cancer progression in the prostate. PLoS Biol. *1*, E59.

Wang, H., Morita, M., Yang, X., Suzuku, T., Yang, W., Wang, J., Ito, K., Wang, Q., Zhao, C., Bartlam, M., et al. (2010). Crystal structure of the human CNOT6L nuclease domain reveals strict poly(A) substrate specificity. EMBO J. *29*, 2566–2576.

Wyles, J.P., McMaster, C.R., and Ridgway, N.D. (2002). Vesicle-associated membrane protein-associated protein-A (VAP-A) interacts with the oxysterol-binding protein to modify export from the endoplasmic reticulum. J. Biol. Chem. *277*, 29908–29918.

Xiao, C., Srinivasan, L., Calado, D.P., Patterson, H.C., Zhang, B., Wang, J., Henderson, J.M., Kutok, J.L., and Rajewsky, K. (2008). Lymphoproliferative disease and autoimmunity in mice with increased miR-17-92 expression in lymphocytes. Nat. Immunol. *9*, 405–414.

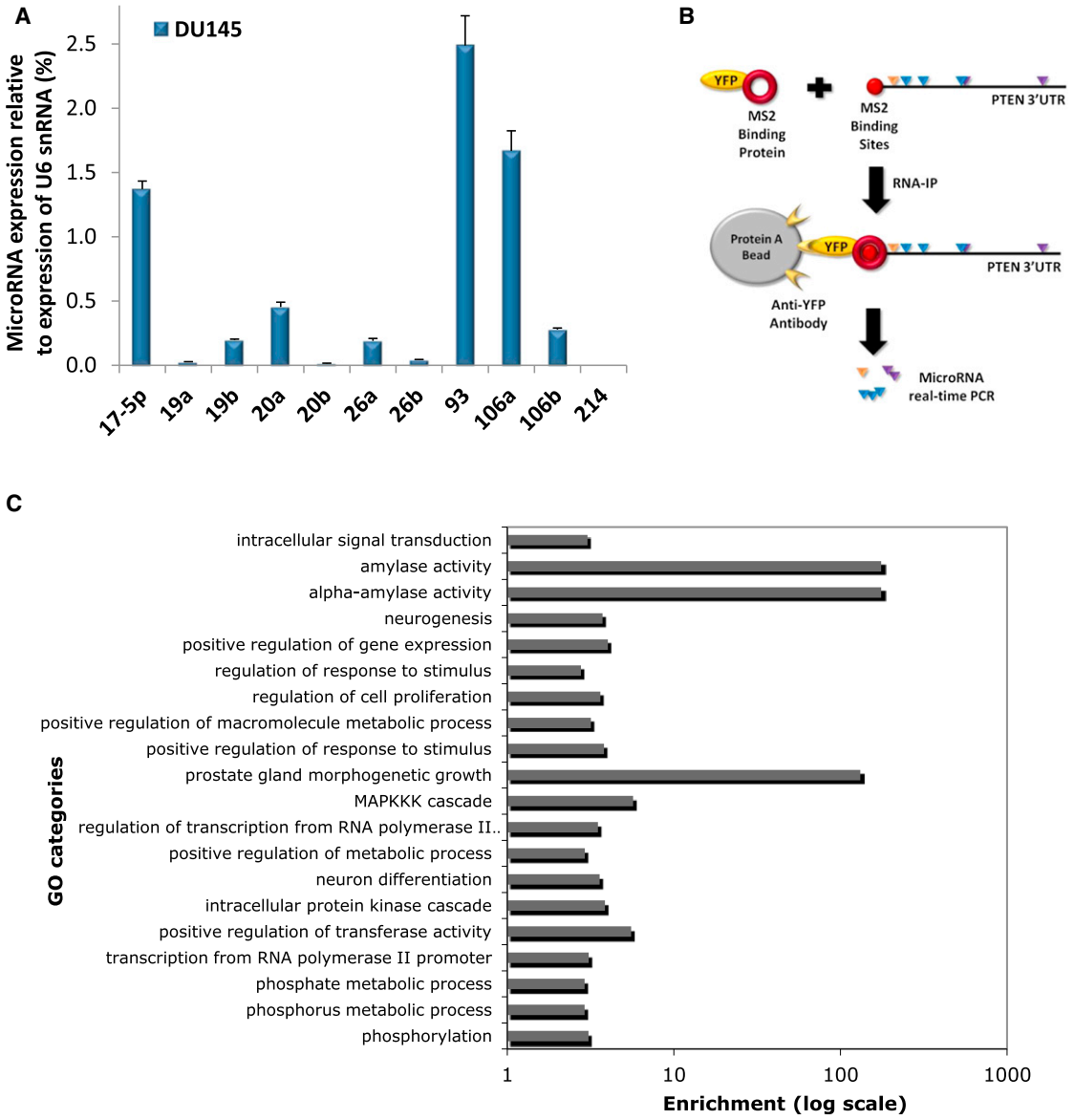

Figure S1. Mutually Targeted MRE Enrichment Analysis Predicts Competitive Endogenous RNAs for PTEN, Related to Figure 1

(A) Expression of PTEN-targeting microRNAs. MicroRNA RT-PCR displaying expression of PTEN-targeting microRNAs in DU145 and HCT116 cells. Mean ± SD; $n \geq 3$.

(B) Schematic outlining the MS2-RNA Immunoprecipitation (RIP) strategy to validate endogenous microRNA:PTEN binding.

(C) Gene ontology analysis of putative PTEN ceRNAs. Graph depicts the 20 most significantly enriched GO categories found in the complete list of predicted PTEN ceRNAs. The enrichment, based on hypergeometric distribution (p value cut-off 0.001), was evaluated for those GO categories with no more than 2000 genes associated (annotation from the Gene Ontology project). The ratio between the number of genes associated to the GO category found in the list and the number of genes expected by chance is reported on x-axes.

A

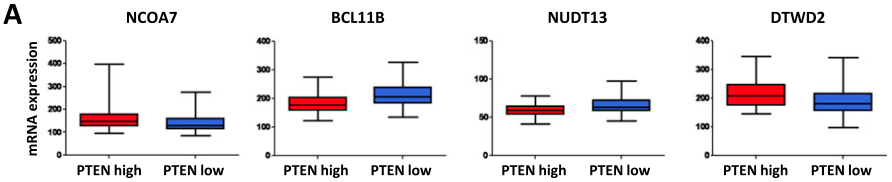

B

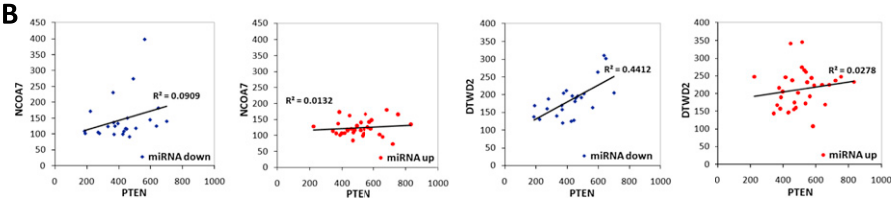

C

Gene	Prostate								Glioblastoma			
	PTEN high/low		PTEN correlation						PTEN high/low		PTEN correlation	
	All samples		All samples		miRNA down		miRNA up		All samples		All samples	
	logFC	T-test	Pearson	P-value	Pearson	P-value	Pearson	P-value	logFC	T-test	Pearson	P-value
NCOA7	-0.22	0.00	0.32	0.00	0.30	0.08	0.11	0.27	-0.55	0.04	0.45	0.00
BCL11B	0.24	0.00	-0.32	0.00	-0.84	0.00	-0.49	0.00	-0.24	0.29	0.13	0.21
SERINC1	-0.28	0.00	0.55	0.00	0.78	0.00	0.49	0.00	-0.53	0.01	0.52	0.00
ZNF460	-0.18	0.00	0.34	0.00	0.63	0.00	0.35	0.02	-0.34	0.00	0.61	0.00
NUDT13	0.15	0.00	-0.43	0.00	-0.62	0.00	-0.35	0.03	-0.35	0.07	0.24	0.07
DTWD2	-0.18	0.00	0.19	0.01	0.66	0.00	0.17	0.18	0.12	0.17	-0.19	0.12
VAPA	-0.16	0.00	0.50	0.00	0.93	0.00	0.74	0.00	-0.65	0.00	0.73	0.00
CNOT6L	-0.51	0.00	0.60	0.00	0.89	0.00	0.64	0.00	-0.73	0.00	0.65	0.00

D

Gene	Prostate	
	Pearson	P-value
MEF2A	0.74	0.00
CNOT6L	0.65	0.00
NBN	0.56	0.00
VAPB	0.55	0.00
NUPL1	0.52	0.00

Gene	Glioblastoma	
	Pearson	P-value
NBR1	0.74	0.00
KCNA7	0.74	0.00
CNOT6L	0.73	0.00
NBN	0.72	0.00
AGPAT5	0.69	0.00

Gene	Correlation	
	Conserved	Human
CNOT6L	3	9
MEF2A	3	8
NUPL1	0	7
NBR1	2	5
NBN	0	5

E

Gene name	Entrez ID	Conserved correlation	Single_species correlation	Pearson coefficient	P value
SERINC1	57515		Ovary	0.8737	1.70E-12
ZNF460	10794		Heart	0.8269	0.000143
			Lung	0.9737	9.53E-08
VAPA	9218		Embryonic tissues	0.7251	2.07E-16
			Stem cells	0.9610	2.02E-19
			Tumor cell lines	0.3953	6.89E-25
			Liver	0.7624	3.05E-10
			Lymphatic tissues	0.6285	0.003952
CNOT6L	246175	All samples	All samples	0.3550	6.91E-154
		Brain-nervous system	Brain-nervous system	0.3076	5.48E-13
		Normal tissues	Normal tissues	0.5220	2.47E-82
			Stem cells	0.9154	3.43E-14
			Tumor cell lines	0.5279	2.76E-46
			Lung	0.6714	0.016818
			Lymphatic tissues	0.8865	4.33E-07
			Ovary	0.7641	3.74E-08
			Testis	0.8457	0.004075

Figure S2. Coexpression of Predicted PTEN ceRNAs in Human Prostate Cancer and Glioblastoma, Multitissue and Normal Tissue-Specific Human-Mouse Conserved, and Human-Specific Coexpression Networks, Related to Figure 2

(A) Comparison of NCOA7, BCL11B, NUDT13 and DTWD2 expression levels in primary prostate cancer between two subsets of samples: "PTEN high" and "PTEN low," classified according to the average PTEN expression level in primary prostate cancer. The ends of the whiskers represent the minimum and maximum of all the data. P values are reported in (C).

(B) Co-expression analysis of PTEN and predicted PTEN ceRNAs NCOA7 and DTWD2 in subsets of human prostate cancer samples with decreased (blue) or increased (red) expression of PTEN-targeting microRNAs. P values are reported in (C).

(C) Summary of the co-expression analysis and corresponding statistical significance of the top 7 predicted PTEN ceRNAs with PTEN in prostate cancer and glioblastoma.

(D) Summary of the correlation analysis between PTEN and the candidates on our list with the 20 lowest MuTaME scores. Of these 20 genes, the top 5 which demonstrate significant correlation with PTEN expression are shown for prostate cancer (left panel), glioblastoma (middle panel) and the co-expression networks (right panel).

(E) Table showing multi-tissues and normal-tissue-specific human-mouse conserved and human-specific co-expression networks where PTEN is found co-expressed with its ceRNA genes. Both multi-tissues and tissue-specific networks were generated by selecting samples corresponding to the chosen category from the complete database (Piro et al., 2011). Pearson coefficients and P values are reported for each relationship found.

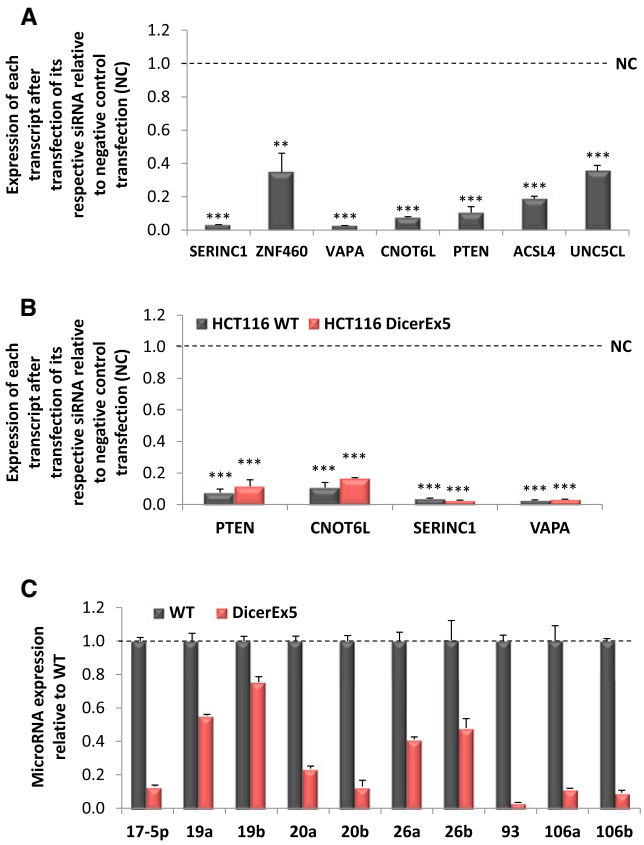

Figure S3. Validation of PTEN ceRNAs, Related to Figure 3

(A and B) Analysis of knock-down efficiency. RT-PCR analysis of PTEN ceRNA expression in response to transfection of (A) DU145 and (B) HCT116 WT and DICER^{Ex5} cells with siRNA against PTEN ceRNAs and selected non-targeting controls.

(C) MicroRNA RT-PCR showing expression of PTEN-targeting microRNAs in WT and DICER^{Ex5} HCT116 cells.

(A–C) Mean ± s.d., n ≥ 3, **p < 0.01; ***p < 0.001.

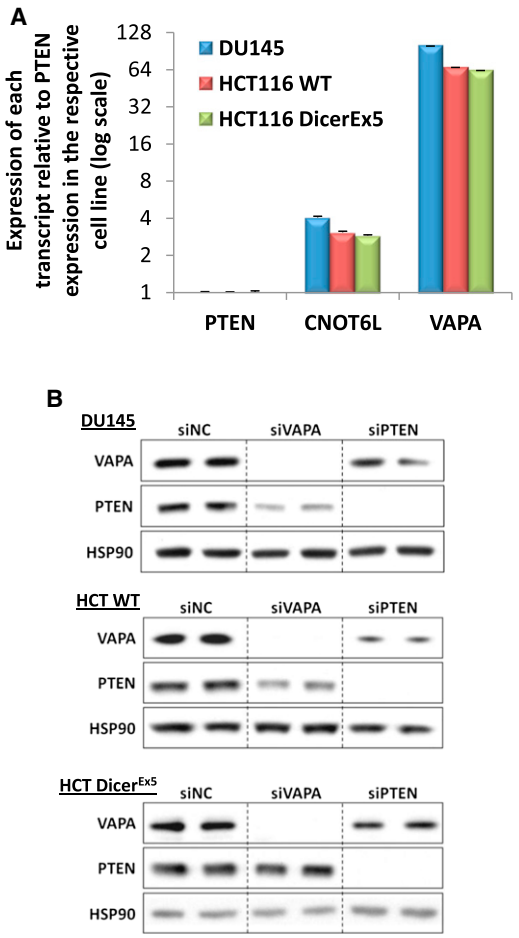

Figure S4. Reciprocal ceRNA Interactions, Related to Figures 4 and 5

(A) RT-PCR analysis showing expression of PTEN ceRNAs relative to PTEN in DU145, HCT116 WT and HCT116 DICER$^{-/-}$ cells. Mean ± s.d., n ≥ 3.

(B) Western blot of PTEN and VAPA protein in DU145, HCT116 WT and HCT116 DICER$^{-/-}$ cells following transfection with siRNAs against VAPA or PTEN.